

## Modelling of recycled aggregate concrete-filled steel tube (RACFST) beam-columns subjected to cyclic loading

You-Fu Yang \*

State Key Laboratory of Coastal and Offshore Engineering, Dalian University of Technology,  
Dalian, 116024, China

(Received February 13, 2012, Revised May 05, 2014, Accepted May 11, 2014)

**Abstract.** A nonlinear finite element analysis (FEA) model is presented for simulating the behaviour of recycled aggregate concrete-filled steel tube (RACFST) beam-columns subjected to constant axial compressive load and cyclically increasing flexural loading. The FEA model was developed based on ABAQUS software package and a displacement-based approach was used. The proposed engineering stress versus engineering strain relationship of core concrete with the effect of recycled coarse aggregate (RCA) replacement ratio was adopted in the FEA model. The predicted results of the FEA model were compared with the experimental results of several RACFST as well as the corresponding concrete-filled steel tube (CFST) beam-columns under cyclic loading reported in the literature. The comparison results indicated that the proposed FEA model was capable of predicting the load versus deformation relationship, lateral bearing capacity and failure pattern of RACFST beam-columns with an acceptable accuracy. A parametric study was further carried out to investigate the effect of typical parameters on the mechanism of RACFST beam-columns subjected to cyclic loading.

**Keywords:** recycled aggregate concrete-filled steel tube (RACFST); finite element analysis (FEA); beam-columns; cyclic loading; bearing capacity; mechanism

---

### 1. Introduction

Recycled aggregate concrete-filled steel tube (RACFST), which causes the recycled aggregate concrete (RAC) to be in a state of protection with the outer steel tube and thus prevents RAC being affected by harmful environmental factors (e.g., wind, moist and temperature), is considered as a new kind of composite structure. Moreover, RACFST can ameliorate the drawbacks and improve the mechanical properties of RAC due to the presence of interactions between steel tube and core RAC. Studies covering the behaviour of RACFST members under various loadings had been carried out, such as static performance under short-term loading (Konno *et al.* 1997, 1998, Mohanraj *et al.* 2011, Yang and Han 2006a, b), time-dependent behaviour under long-term sustained loads (Yang 2011, Yang *et al.* 2008), and seismic performance under cyclic loading (Yang *et al.* 2009, Yang and Zhu 2009). The previous studies indicated that RACFST members

---

\*Corresponding author, Professor, E-mail: [youfuyang@163.com](mailto:youfuyang@163.com)

also possessed good mechanical properties and had the potential for application in new building structures.

There were many studies devoted to the modelling of concrete-filled steel tube (CFST) beam-columns under constant axial compressive load and cyclically increasing flexural loading. Aval *et al.* (2002) presented the method for analysis of CFST beam-columns under cyclic loading based on a comprehensive composite inelastic fibre element, in which the effect of semi- and perfect bond between steel tube and concrete over the entire contact surface was considered. Chung (2010), Han and Yang (2005) and Han *et al.* (2003) introduced the fibre element method for predicting the pre- and post-peak hysteretic behaviour of CFST beam-columns without slip at steel-concrete interface considered. Hajjar *et al.* (1998) proposed a method for cyclic analysis of square and rectangular CFST beam-columns using a three-dimensional fibre-based distributed plasticity finite element. The cyclic model for steel and concrete was based on the stress-space bounding-surface plasticity formulation, and the interlayer slip between steel tube and core concrete was also formulated. Based on ABAQUS software package and fibre analysis technique, Susantha *et al.* (2002) carried out the theoretical modelling of partially concrete-filled steel box beam-columns under cyclic loading using a type of beam-column element (B21) available in the software. A two-node frame element for cyclic analysis of CFST beam-columns was formulated by Valipour and Foster (2010), from which the influence of material nonlinearity, size effect, steel tube confinement and local buckling, and the second-order effect were addressed. A fibre-based model was developed by Varma *et al.* (2002, 2005) for cyclic analysis of square CFST beam-columns with high-strength concrete, and the uniaxial stress versus strain relationship for steel and concrete fibres of CFST cross-section was derived from the three-dimensional nonlinear finite element analysis (FEA) results. To date, no attention has been given to the modelling of RACFST beam-columns under constant axial compressive load and cyclically increasing flexural loading. The lack of information on theoretical model for cyclic analysis of RACFST beam-columns indicates that further research is necessary in this area.

In this study, a nonlinear finite element analysis (FEA) model for predicting the behaviour of RACFST beam-columns under reversed cyclic loading while subjected to constant axial compressive load is developed. The main objectives of this research are thus threefold: first, to present a FEA model that can be used to predict the load versus deformation relationship, lateral bearing capacity and failure pattern of RACFST beam-columns under cyclic loading; second, to verify the results obtained from the FEA model by comparison with the test results; and finally, to investigate the effect of typical parameters on the mechanism of RACFST beam-columns subjected to cyclic loading.

## 2. Summary of the test results

Tests performed by Yang *et al.* (2009) and Yang and Zhu (2009) provided the measured load versus deformation relationship, lateral bearing capacity and typical failure pattern of RACFST and the reference CFST specimens under cyclic loading while subjected to constant axial compressive load. The detailed information of the tested specimens is given in Table 1, where  $D$  is the diameter or overall face width of circular or square steel tube;  $t$  is the wall thickness of steel tube;  $f_y$  is the yield strength of steel;  $f_{cu}$  is the cube compressive strength of concrete;  $N_o$  is the applied axial compressive load;  $n$  is the axial load level, which is defined as  $N_o/N_u$  and  $N_u$  is the bearing capacity of the composite columns under short-term static loading (Yang and Han 2006b);

$P_{ue}$  is the measured lateral bearing capacity; and  $P_{uc}$  is the predicted lateral bearing capacity. The length of specimens is 1500 mm. The test program consists of three series of investigations: eleven specimens with recycled coarse aggregate (RCA) replacement ratio ( $r$ ) of 25% by weight, eleven specimens with  $r$  of 50% by weight and six specimens with normal concrete. The specimens are labeled such that the steel tube shape, axial load level and type of concrete can be identified from the label. The labels used to characterize each specimen are as following: (1) Steel tube shape: circular (C) and square (S); (2) Axial load level: (a)  $n = 0.05$ ; (b)  $n = 0.25$ ; and (c)  $n = 0.43$  to  $0.52$ ; and (3) Type of concrete: normal concrete (0), RAC containing 25% RCA (1) and RAC containing

Table 1 Summary of test information

Section type	Specimen label	$D \times t$ (mm)	$D / t$	$f_y$ (MPa)	$f_{cu}$ (MPa)	$N_o$ (kN)	$n$	$P_{ue}$ (kN)	$P_{uc}$ (kN)	$P_{uc} / P_{ue}$
Circular	Ca0	165 × 2.57	64.2	343.1	60.4	62.8	0.05	94.0	94.7	1.007
	Ca1	165 × 2.57	64.2	343.1	59.2	62.1	0.05	92.8	97.9	1.055
	Ca2	165 × 2.57	64.2	343.1	52.2	57.7	0.05	92.0	98.5	1.071
	Cb0	165 × 2.57	64.2	343.1	60.4	313.9	0.25	106.1	107.9	1.017
	Cb1-1	165 × 2.57	64.2	343.1	59.2	310.3	0.25	102.4	107.6	1.051
	Cb1-2	165 × 2.57	64.2	343.1	59.2	310.3	0.25	103.3	107.6	1.042
	Cb2-1	165 × 2.57	64.2	343.1	52.2	288.7	0.25	98.4	103.2	1.049
	Cb2-2	165 × 2.57	64.2	343.1	52.2	288.7	0.25	100.1	103.2	1.031
	Cc0	165 × 2.57	64.2	343.1	60.4	600.0	0.48	109.0	106.7	0.979
	Cc1-1	165 × 2.57	64.2	343.1	59.2	600.0	0.48	107.9	103.8	0.962
	Cc1-2	165 × 2.57	64.2	343.1	59.2	600.0	0.48	106.3	103.8	0.976
	Cc2-1	165 × 2.57	64.2	343.1	52.2	600.0	0.52	103.4	101.1	0.978
	Cc2-2	165 × 2.57	64.2	343.1	52.2	600.0	0.52	98.0	101.1	1.032
	Square	Sa0	150 × 2.94	51.0	344.4	60.4	69.9	0.05	109.8	107.0
Sa1-1		150 × 2.94	51.0	344.4	59.2	69.1	0.05	106.9	101.5	0.949
Sa1-2		150 × 2.94	51.0	344.4	59.2	69.1	0.05	106.1	101.5	0.957
Sa2-1		150 × 2.94	51.0	344.4	52.2	64.3	0.05	105.3	100.6	0.955
Sa2-2		150 × 2.94	51.0	344.4	52.2	64.3	0.05	105.4	100.6	0.954
Sb0		150 × 2.94	51.0	344.4	60.4	349.7	0.25	124.5	111.6	0.896
Sb1-1		150 × 2.94	51.0	344.4	59.2	345.7	0.25	122.8	107.5	0.875
Sb1-2		150 × 2.94	51.0	344.4	59.2	345.7	0.25	122.9	107.5	0.875
Sb2-1		150 × 2.94	51.0	344.4	52.2	321.4	0.25	119.3	104.6	0.877
Sb2-2		150 × 2.94	51.0	344.4	52.2	321.4	0.25	119.1	104.6	0.878
Sc0		150 × 2.94	51.0	344.4	60.4	600.0	0.43	133.1	116.3	0.874
Sc1-1		150 × 2.94	51.0	344.4	59.2	600.0	0.43	129.8	112.7	0.868
Sc1-2		150 × 2.94	51.0	344.4	59.2	600.0	0.43	129.3	112.7	0.872
Sc2-1		150 × 2.94	51.0	344.4	52.2	600.0	0.47	127.6	110.3	0.864
Sc2-2	150 × 2.94	51.0	344.4	52.2	600.0	0.47	127.2	110.3	0.867	

50% RCA (2). For example, the label “Cb1-1” indicates that the specimen is the first circular composite column with RAC containing 25% RCA and its axial load level is 0.25.

The tube of the tested specimens was cut from long cold-formed hollow steel sections. The properties of steel were obtained by tensile coupon tests, and the results were given in Yang *et al.* (2009) and Yang and Zhu (2009). Three types of concrete were produced, i.e., RAC with  $r$  of 25% and 50%, and normal concrete with natural aggregates. RAC was produced by replacing 25% or 50% of natural coarse aggregate with RCA. The source and property of RCA were detailed in Yang and Han (2006a, b). The properties of concrete were determined from standard 150 mm cube and 150 mm  $\times$  300 mm prism tests and the results were presented in Yang *et al.* (2009) and Yang and Zhu (2009).

The specimens were tested under combined constant axial compressive load and cyclically increasing flexural loading. The axial compressive load ( $N_o$ ) was applied and maintained constant by a 1000 kN hydraulic ram. The flexural loading was applied by imposing cyclically lateral forces (displacements) in the middle of the specimen via a MTS load cell having 250 kN capacity, as shown in Fig. 1. Displacement transducers and strain gauges (SG) were used to measure the in-plane displacements and strains respectively, and the out-of-plane deformation of specimens was prevented by four lateral braces. The arrangements of stain gauge (SG) are illustrated in Fig. 2. The tests were continued until either the specimen failed due to the fracture of steel tube or the lateral load resistance of specimen had deteriorated to 50% of the lateral bearing capacity.

### 3. Finite element analysis (FEA) model

To analyse the behaviour of RACFST beam-columns subjected to constant axial compressive load and cyclically increasing flexural loading, a three-dimensional nonlinear finite element analysis (FEA) model was developed using ABAQUS software package (2007).

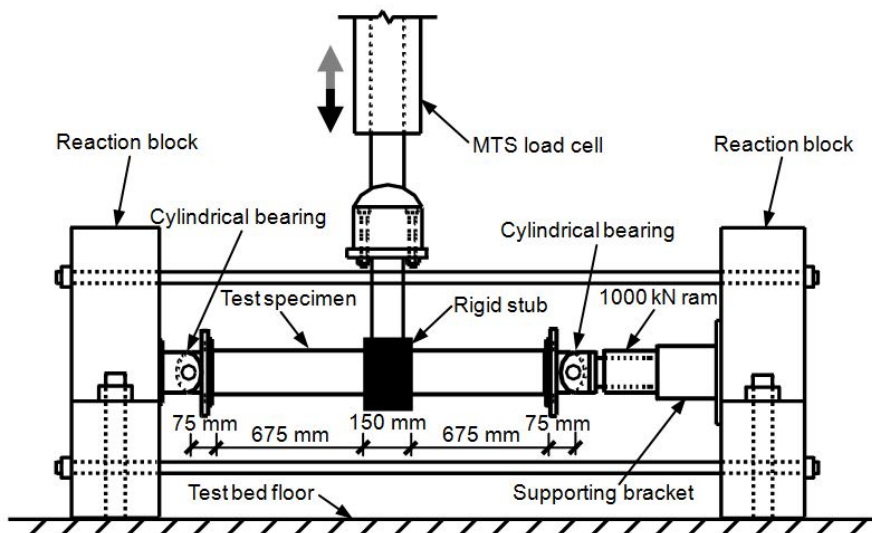


Fig. 1 Outline of test setup

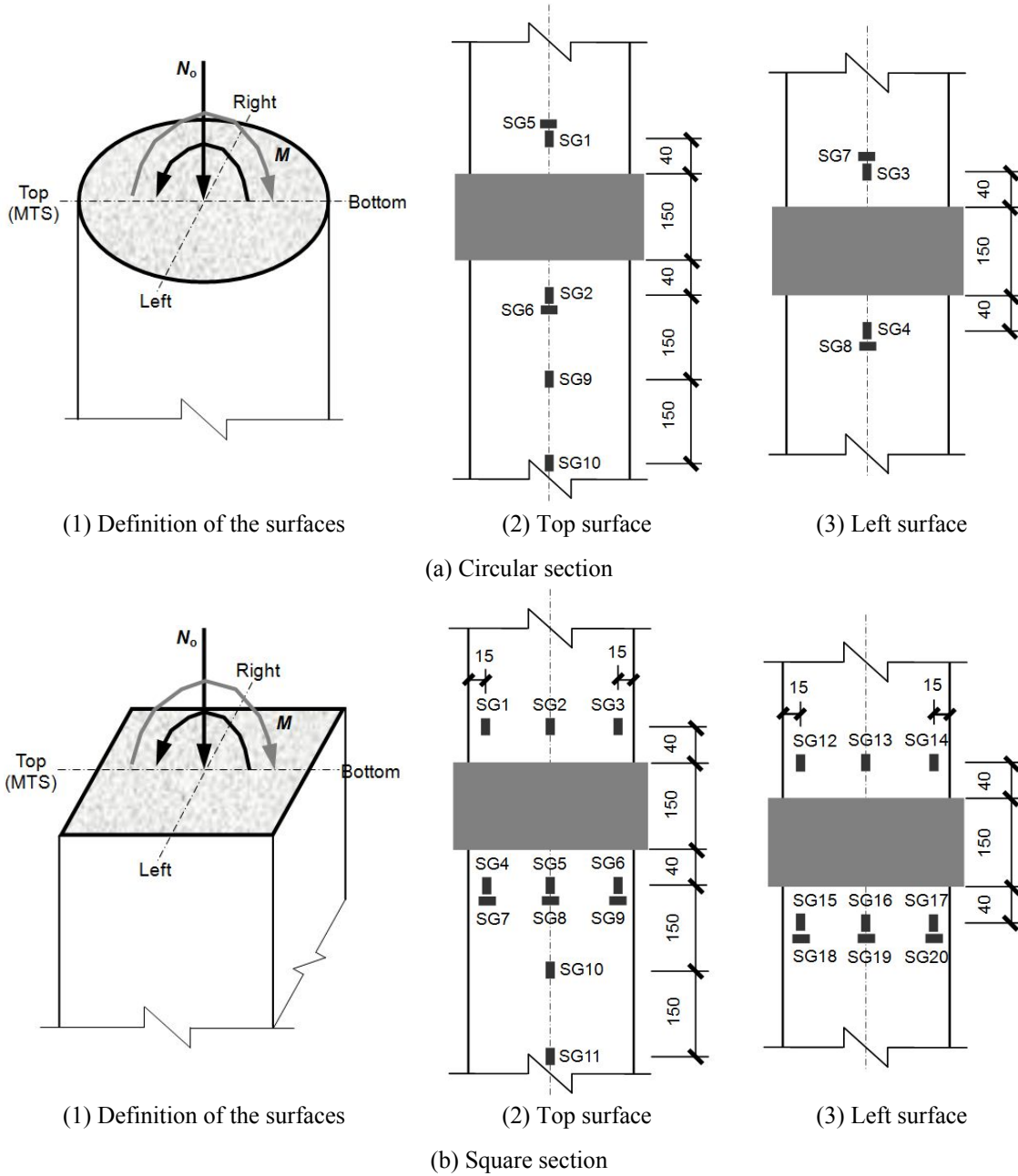


Fig. 2 Arrangements of strain gauge (SG) (unit: mm)

### 3.1 Material models

To simulate the mechanical behaviour of structural steel under cyclic loading, a nonlinear kinematic hardening model in ABAQUS (2007) was adopted. It is assumed that the yielding of

steel is independent of the equivalent pressure stress and the slope at hardening stage changes after the nominal stress greater than yielding point. The model uses Mises yield surfaces with associated plastic flow, which allows for isotropic yielding, and the Bauschinger effect and plastic shakedown are also considered. The nonlinear relationship of true stress versus logarithmic plastic true strain is required to be defined for steel component, which can be converted from the engineering stress versus engineering strain relationship (ABAQUS 2007). An elastic-plastic model was adopted to describe the engineering stress-strain relationship of steel, and the hardening modulus was taken as  $0.05 E_s$ , where  $E_s$  is the elastic modulus of steel. For cold-formed square steel tube, the corner effect was taken into account based on the formulae suggested by Abdel-Rahman and Sivakumaran (1997).

The damaged plasticity model in ABAQUS (2007) was used to model the complicate nonlinear behaviour of RAC under cyclic loading. The model takes into consideration the degradation of elastic stiffness induced by plastic straining both in tension and compression. The degradation of the elastic stiffness of concrete is characterized by two damage variables (i.e., tension degradation factor  $d_t$  and compression degradation factor  $d_c$ ), which are assumed to be the function of the plastic strains, temperatures and field variables. Through pilot calculations, it is shown that the convergence cannot be easily achieved using the method in ABAQUS (2007) and the equations suggested by Birtel and Mark (2006) are adopted to calculate the damage variables ( $d_t$  and  $d_c$ ). Furthermore, the stiffness recovery during the elastic unloading process from tension to compression is used to consider the opening and closing of micro cracks in concrete. The compression stiffness recovery factor ( $w_c$ ) and the tension stiffness recovery factor ( $w_t$ ) were set to be 0.2 and 0.0, respectively.

The model assumed that the tensile and compressive responses of concrete were characterized by damaged plasticity. For RAC under compression, the plastic performance came from the engineering stress versus engineering strain relationship and the uniaxial engineering stress-strain relationship needed to be converted into stress versus plastic strain relationship. The investigation carried out on RACFST stub columns under axial compression (Yang and Han 2006a) showed that, the behaviour of core RAC was similar to that of core concrete in CFST; however, the shape of engineering stress-strain curve of RAC was obviously determined by RCA replacement ratio ( $r$ ).

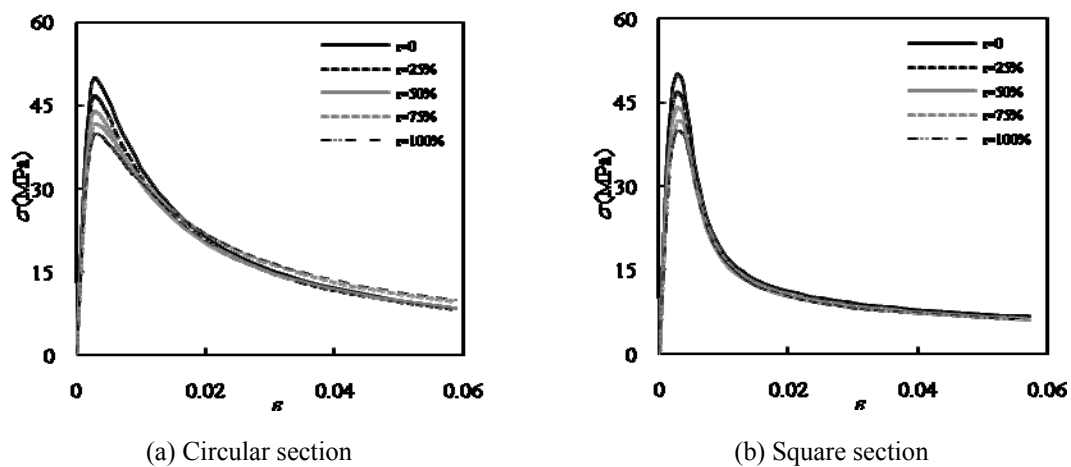


Fig. 3 Typical engineering stress-strain relationship of RAC under compression

The uniaxial engineering stress-strain relationship with the effect of  $r$  had been proposed as follows (Yang 2007)

$$y = \begin{cases} 2x - x^2 & (x \leq 1) \\ x / [\beta_0 \cdot (x-1)^\eta + x] & (x > 1) \end{cases} \quad (1)$$

in which,  $x = \varepsilon / \varepsilon_0$ ,  $y = \sigma / \sigma_0$ .

$$\begin{aligned} \sigma_0 &= f'_{c,r} = f'_c \cdot (1 - 0.28r + 0.08r^2); \\ \varepsilon_0 &= (1300 + 12.5f'_c + 800\xi^{0.2}) \cdot [1 + r / (65.715r^2 - 109.43r + 48.989)] \times 10^{-6}; \\ \eta &= \begin{cases} 2 & \text{(Circular section)} \\ 1.6 + 1.5/x & \text{(Square section)} \end{cases}; \\ \beta_0 &= \begin{cases} 0.5(f')^{0.5} \cdot (2.36 \times 10^{-5})^{[0.25 + (\xi_r - 0.5)^7]} \geq 0.12 & \text{(Circular section)} \\ (f')^{0.1} / (1.2\sqrt{1 + \xi_r}) & \text{(Square section)} \end{cases}. \end{aligned}$$

where,  $f'_{c,r}$  and  $f'_c$  are the cylinder compressive strength of RAC and the corresponding normal concrete, respectively;  $\xi_r (= \alpha \cdot f'_y / f_{ck,r})$  is the confinement factor of RACFST, in which  $\alpha = A_s / A_c$  is the steel ratio,  $A_s$  and  $A_c$  are the cross-sectional area of steel and concrete respectively,  $f_{ck,r}$  is the characteristic strength of RAC and equals to 0.67% of the cube compressive strength of RAC (Yang 2011);  $\xi$  is the confinement factor of CFST (Han and Yang 2005, Han *et al.* 2003). The correspondence between cube and cylinder compressive strength of concrete in EN 1992-1-1 (2004) is temporarily adopted in this paper. The typical engineering stress-strain relationship of RAC under compression is illustrated in Fig. 3. The basic calculating conditions are:  $\alpha = 0.1$ ,  $f'_y = 345$  MPa and  $f'_c = 50$  MPa.

For RAC under tension, the tension stiffening effect related to strain was adopted to describe the plastic performance, and the tensile stress versus cracking strain relationship suggested by Birtel and Mark (2006) was selected as the input data for ABAQUS (2007). In the prediction, the elastic modulus of concrete was the initial tangent modulus of engineering stress-strain curve, and the Poisson's ratio of concrete was set to be 0.2.

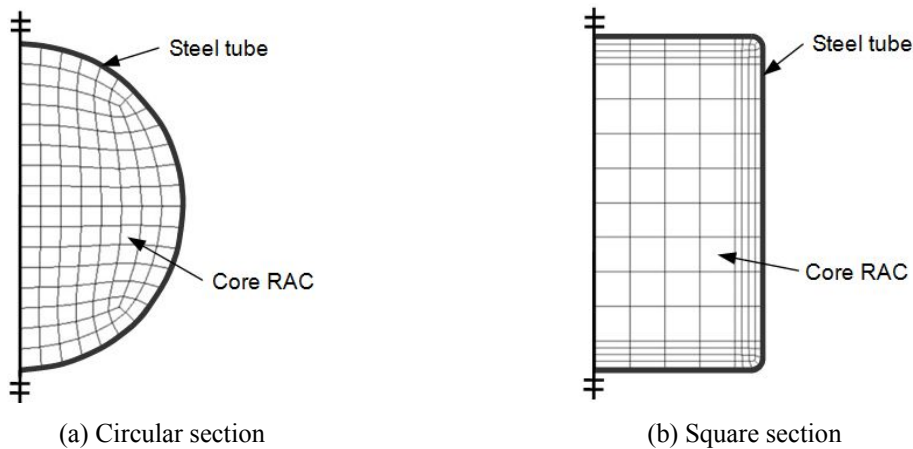


Fig. 4 Meshing of cross-section

### 3.2 Element types and meshing

The steel tube was simulated by four-node fully integrated shell elements (S4), and the Simpson integration with 9 integration points along the thickness of shell was used. Core RAC and endplate were simulated by eight-node reduced-integration three-dimensional brick elements (C3D8R).

The structured meshing in ABAQUS (2007) was adopted and the mesh size in three dimensions did not vary too much to ensure the accuracy of the prediction. Moreover, the meshing tests were performed to get the reasonable results by the time as little as possible. At the corner part of cold-formed square steel tube, the tube and core RAC were meshed with smaller sizes than other parts. Fig. 4 demonstrates the meshing of cross-section.

### 3.3 Contact models and boundary conditions

Currently, there is no literature related to the bond performance between steel tube and core RAC. The failure pattern of core concrete in RACFST specimens showed that no obvious bond failure between RAC and steel tube was observed, as presented in Yang *et al.* (2009) and Yang and Zhu (2009) and demonstrated in Fig. 5. As a result, the contact models in ABAQUS (2007), which were successfully used in the modelling of CFST members (Han *et al.* 2008, 2007), were adopted to simulate the interaction between steel tube and core RAC under cyclic loading. In the normal direction, a contact pressure model containing gap element with big gap rigidity was used, and in the tangential directions a Coulomb friction model with the friction coefficient of 0.25 was adopted. The interaction between endplate and core RAC was simulated using the contact pressure model only in the normal direction, and the ‘tie contact’ in ABAQUS (2007) was selected to model the contact between steel tube and endplate.

It should be noted that, the endplate was relatively thin compared with the length of column, and the influence of endplate on the global deformation of column can be neglected. Thus, the endplate was replaced by the rigid plate in the modelling, and the elastic modulus and Poisson’s ratio of the rigid plate were set to be  $1.0 \times 10^{12}$  N/mm<sup>2</sup> and 0.001, respectively. The symmetry was considered and one-fourth of the column was simulated while subjected to constant axial compressive load and cyclically increasing flexural loading. The boundary conditions in the



Fig. 5 Typical failure pattern of core concrete

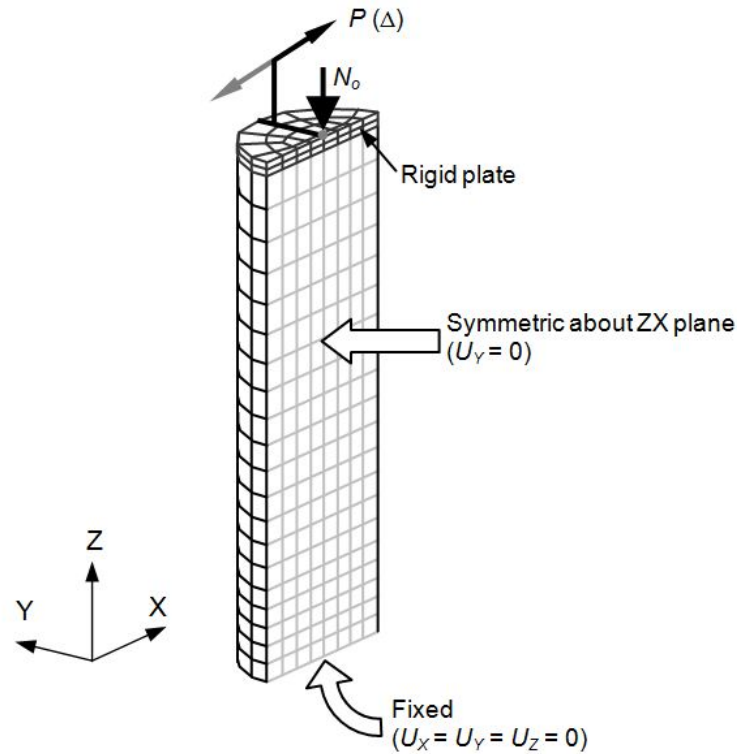
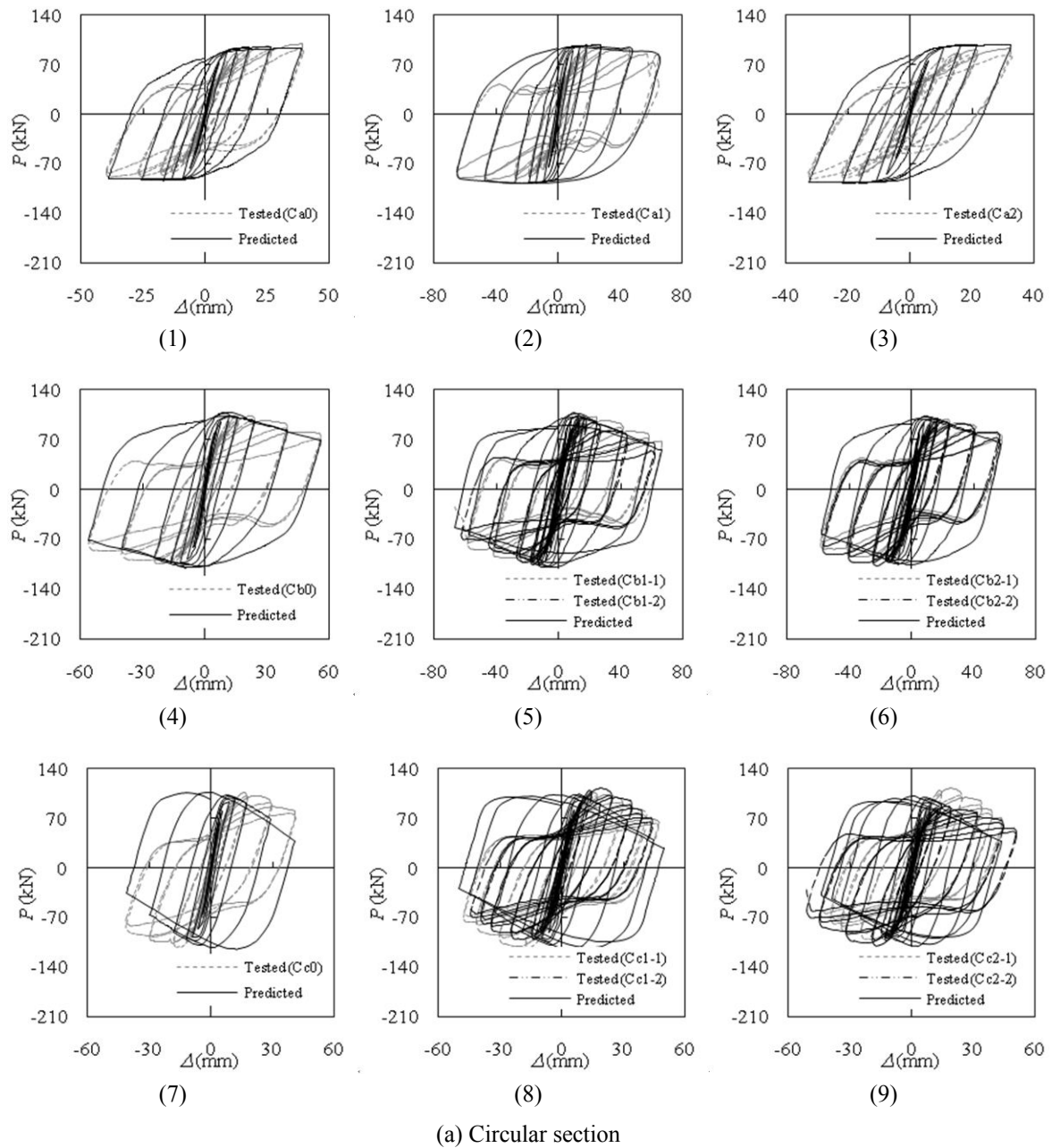


Fig. 6 Boundary conditions

modelling are shown in Fig. 6. The constant axial compressive load was applied at the central point of the top rigid plate firstly, and then the lateral displacements ( $\Delta$ ) were applied to the symmetry line of the top rigid plate in accordance with the loading histories in the tests (Yang *et al.* 2009, Yang and Zhu 2009). The responses of the composite beam-columns under cyclic loading after each step were calculated from the equilibrium equations, and the well-known Newton-Raphson incremental iterative solution method was used.

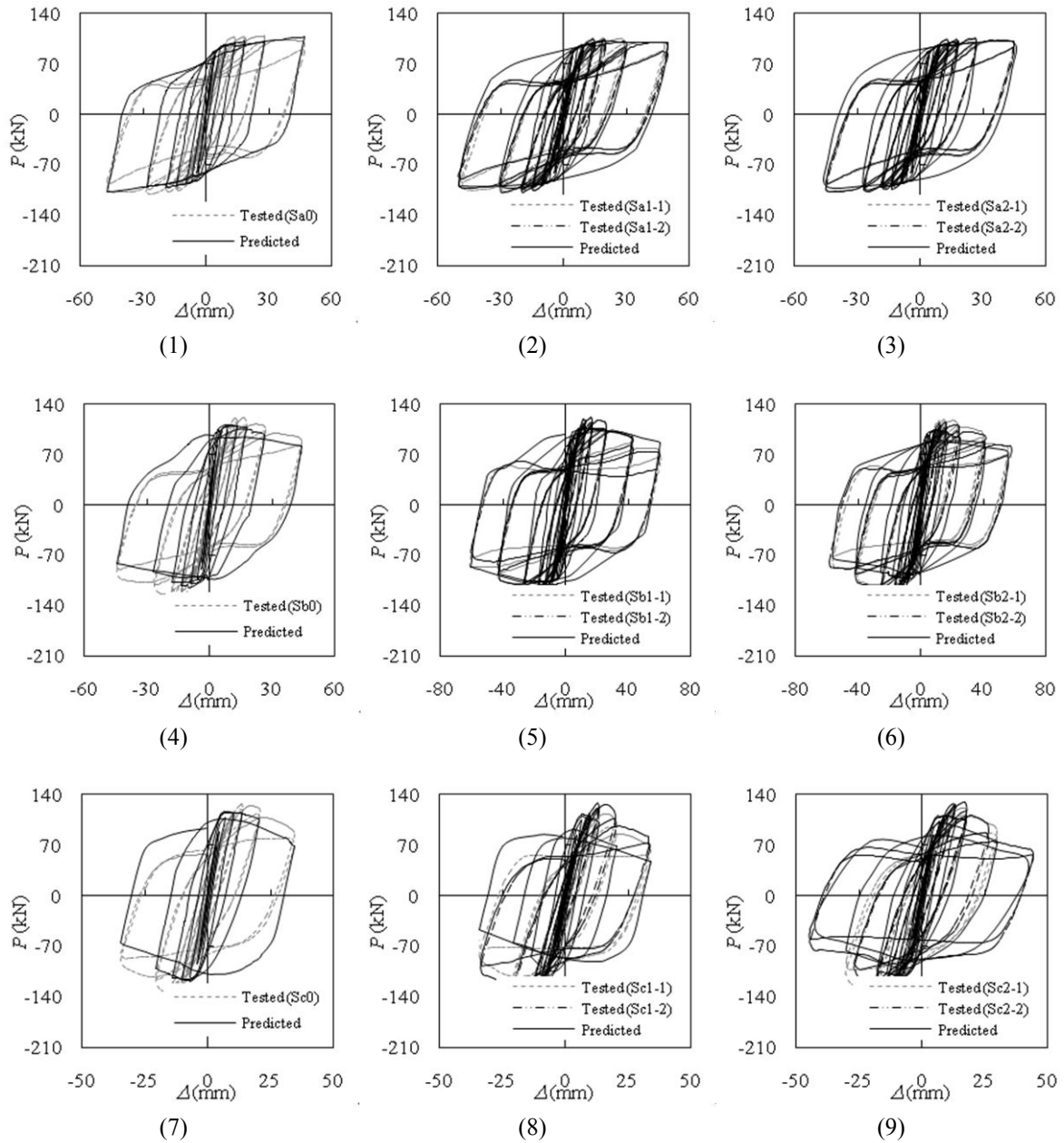
### 3.4 Verification of FEA model

The predicted hysteretic curves of lateral load ( $P$ ) versus lateral displacement ( $\Delta$ ) using the FEA model are compared with the test results of RACFST and the corresponding CFST beam-columns under cyclic loading (Yang *et al.* 2009, Yang and Zhu 2009), as shown in Fig. 7, and the calculated lateral bearing capacities ( $P_{uc}$ ) are presented in Table 1. The last column of Table 1 shows the comparison between  $P_{uc}$  and  $P_{ue}$ , and a mean of 0.957 and a standard deviation of 0.071 of  $P_{uc}/P_{ue}$  are obtained. It can be seen that, generally, a good agreement is obtained between the predicted and measured results. The predicted skeleton curves and initial unloading stiffness agree well with the measured results of hysteretic  $P - \Delta$  curves; however, at the latter part of the descent stage of hysteretic  $P - \Delta$  curves, there are actually certain differences between the predicted and tested results. This may be induced by the unexpected initial eccentricity in the tests, which enhances the influence of second-order effect.



(a) Circular section  
 Fig. 7 Comparison of hysteretic  $P-\Delta$  curve between predicted and tested results

Fig. 8 shows the comparison between predicted and measured typical hysteretic lateral load ( $P$ ) versus strain ( $\epsilon$ ) curves. It can be observed that the predicted  $P - \epsilon$  curves of circular specimens (Fig. 8(a)) are generally in good agreement with the test results; however, the predicted  $P - \epsilon$  curves of square specimens (Fig. 8(b)) are lower than the measured results. This may be explained by that, due to the weaker confinement of square steel tube to core concrete, the effect of the



(b) Square section

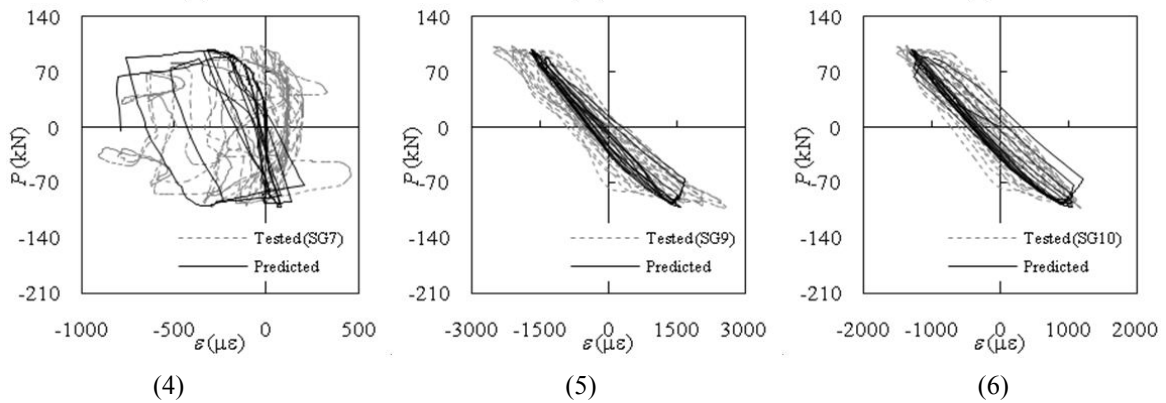
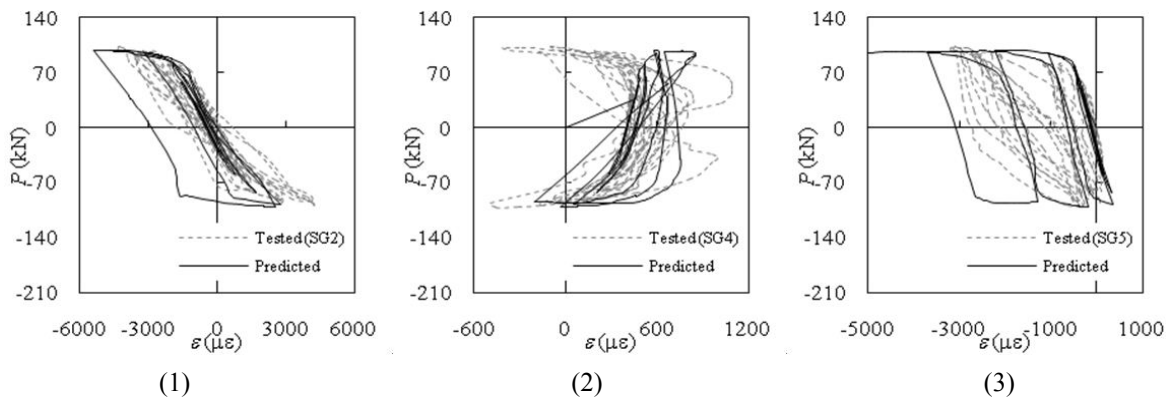
Fig. 7 Continued

unexpected initial imperfections on square specimens is greater compared with circular specimens.

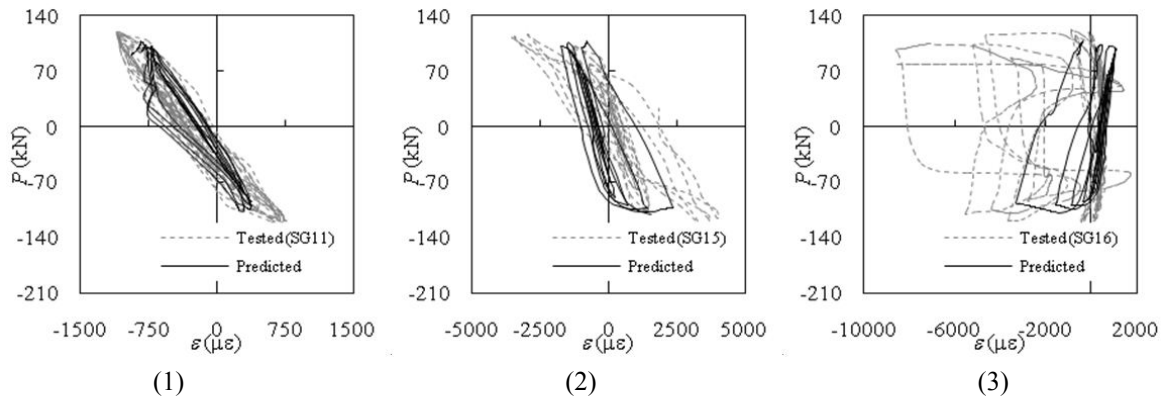
Fig. 9 demonstrates the comparison of typical failure pattern between predicted and measured results. It can be seen that, in general, the predicted failure pattern and buckling position of steel tube accord well with the test results.

3.5 Effect of typical parameters on monotonic  $P-\Delta$  curves

Fig. 10 shows the comparison between the calculated hysteretic and monotonic  $P-\Delta$  curve. It can be seen that, the monotonic  $P-\Delta$  curve is so close to the skeleton curve of the hysteretic  $P-\Delta$  relationship.



(a) Specimen Cb1-1



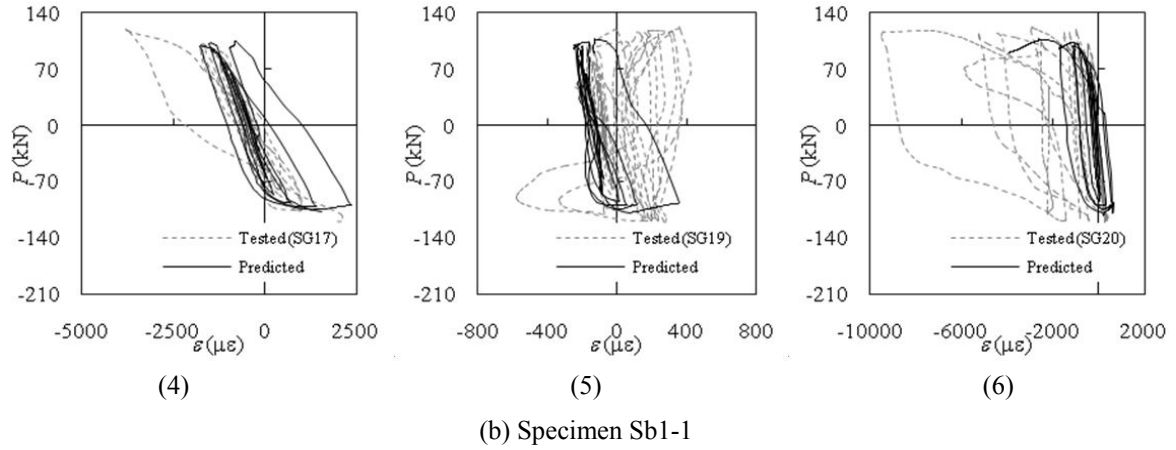


Fig. 8 Comparison of typical hysteretic  $P - \varepsilon$  curves

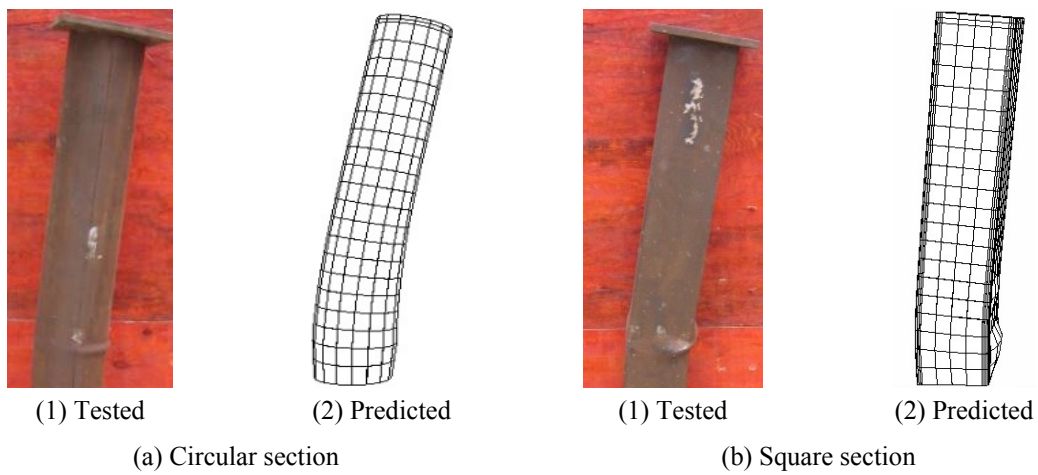


Fig. 9 Comparison of typical failure pattern

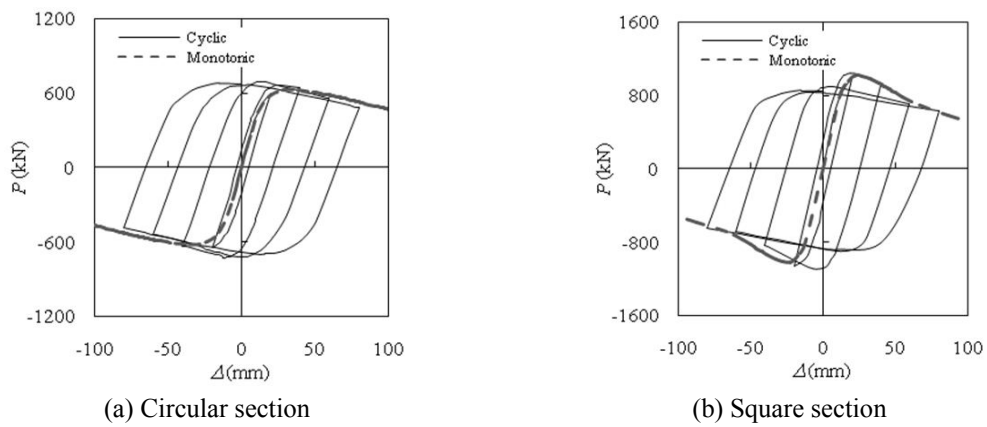


Fig. 10 Comparison between hysteretic and monotonic  $P - \Delta$  curve

Based on the FEA model, the influence of RCA replacement ratio ( $r$ ), cylinder compressive strength of normal concrete ( $f'_c$ ), yield strength of steel ( $f_y$ ), steel ratio ( $\alpha$ ), slenderness ratio ( $\lambda, = 4L/D$  for circular column and  $= 2\sqrt{3}L/D$  for square column, and  $L$  is the effective buckling length of column in the plane of bending), and axial load level ( $n$ ) on monotonic  $P - \Delta$  curve of RACFST beam-columns was investigated, and the results are demonstrated in Fig. 11. The calculating conditions include:  $D = 400$  mm,  $f_y = 345$  MPa,  $f'_c = 50$  MPa,  $\alpha = 0.1$ ,  $n = 0.4$ ,  $\lambda = 40$  and  $r = 50\%$ . The calculated lateral bearing capacity ( $P_u$ ) and initial slope ( $K_s$ ) of RACFST beam-columns under different parameters are presented in Table 2. It can be seen from Fig. 11 and Table 2 that, circular and square members have the similar  $P - \Delta$  responses under the same conditions; however, due to the weaker confinement to core concrete, the decrease of load after reaching the bearing capacity of square columns is faster than that of circular columns. In general, similar to CFST beam-columns under cyclic loading (Han and Yang 2005, Han *et al.* 2003),  $K_s$  of  $P - \Delta$  curves increases with increase of  $\alpha$  and decrease of  $\lambda$  and  $n$ , and other parameters, such as  $r$ ,  $f'_c$  and  $f_y$ , have a moderate effect on  $K_s$ .  $P_u$  of RACFST beam-columns increases with increase of  $f'_c$ ,  $f_y$  and  $\alpha$ , and decrease of  $r$  and  $\lambda$ . Moreover,  $P_u$  of circular RACFST beam-columns generally decreases with increase of  $n$ ; however, for square RACFST beam-columns,  $P_u$  increases with increase of  $n$  when  $n$  is less than or equal to 0.3, and decreases with increase of  $n$  when  $n$  is greater than 0.3.

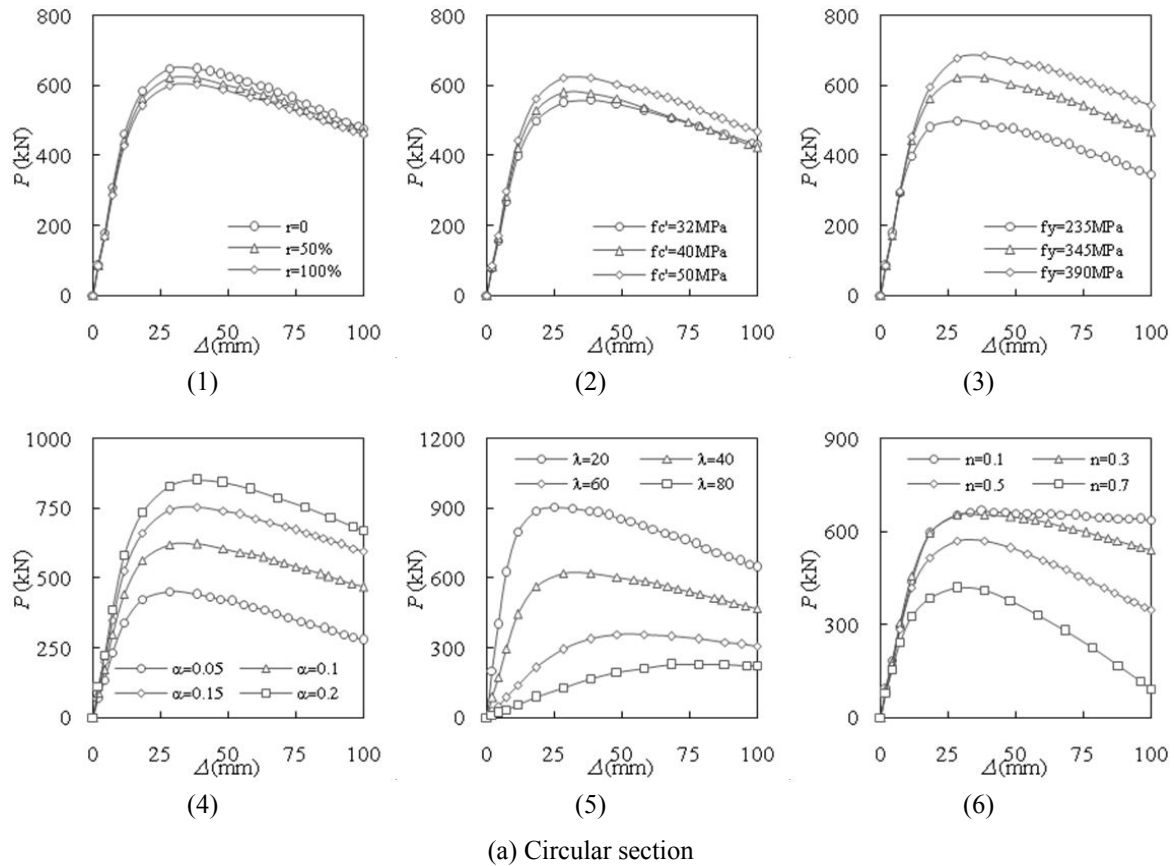
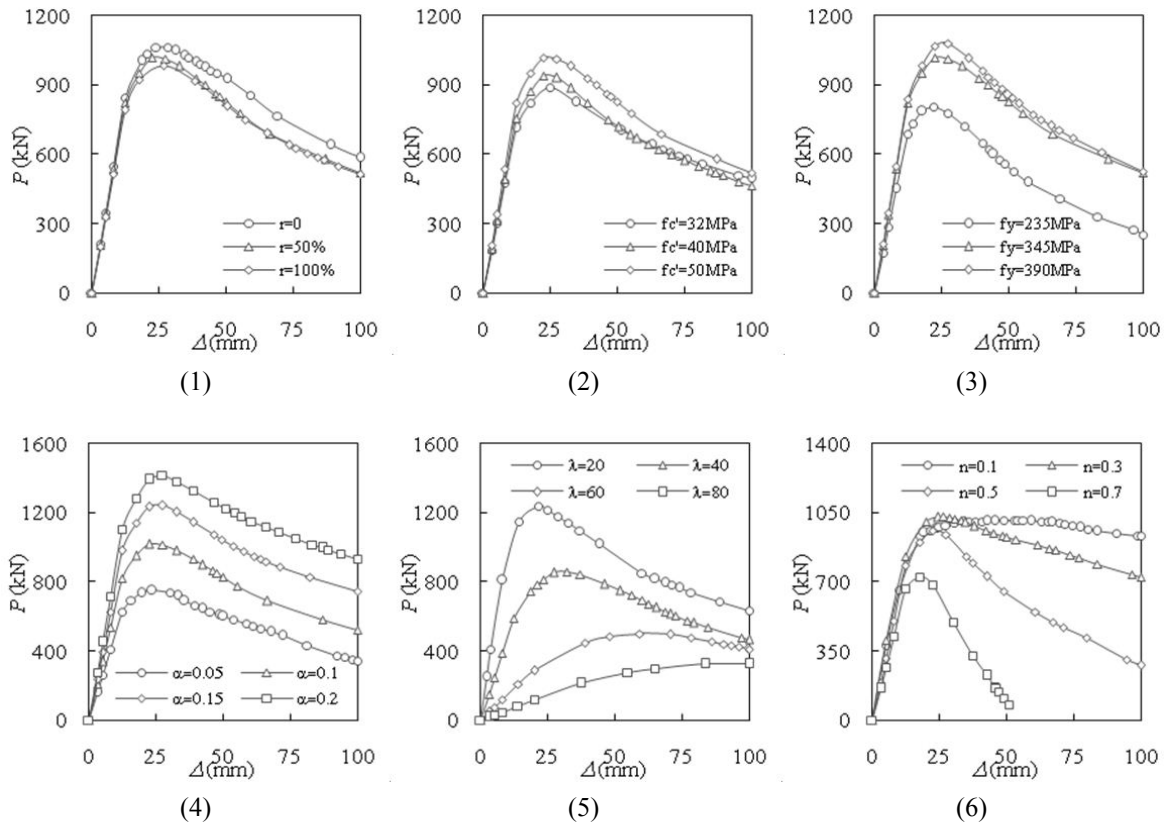


Fig. 11 Effect of typical parameters on monotonic  $P - \Delta$  curve



(b) Square section

Fig. 11 Continued

Table 2 Calculated results of RACFST beam-columns under different parameters

Section type	Parameter	$P_u$ (kN)	$K_s$ (kN/mm)	$p_{B,1}$ (MPa)	$p_{B,3}$ (MPa)	
Circular	$r$	0	647.5	45.4	0.24	2.11
		50%	621.8	43.8	1.05	3.22
		100%	602.6	42.3	1.13	3.07
	$f'_c$ (MPa)	32	557.1	39.6	1.33	2.99
		40	579.1	41.5	0.87	2.09
		50	621.8	43.8	1.05	3.22
	$f_y$ (MPa)	235	499.8	45.1	0.00	1.72
		345	621.8	43.8	1.05	3.22
		390	685.3	43.8	1.06	3.44
	$\alpha$	0.05	452.9	35.0	0.01	1.10
		0.1	621.8	43.8	1.05	3.22
		0.15	755.1	51.0	2.09	4.03
0.2		850.1	56.6	2.82	4.25	

Table 2 Continued

Section type	Parameter	$P_u$ (kN)	$K_s$ (kN/mm)	$p_{B,1}$ (MPa)	$p_{B,3}$ (MPa)	
Circular	$\lambda$	20	905.4	102.6	3.12	5.45
		40	621.8	43.8	1.05	3.22
		60	358.1	12.5	0.45	1.72
		80	230.4	4.8	0.00	1.00
	$n$	0.1	664.6	50.6	0.00	5.59
		0.3	654.0	45.3	0.00	2.73
		0.5	570.0	42.8	1.41	2.62
		0.7	416.9	42.2	1.53	2.03
Square	$r$	0	1061.8	72.7	0.75	2.35
		50%	1018.1	71.0	1.07	1.96
		100%	984.5	68.6	1.24	3.30
	$f'_c$ (MPa)	32	887.1	63.1	1.96	2.92
		40	939.0	65.7	1.39	2.41
		50	1018.1	71.0	1.07	1.96
	$f_y$ (MPa)	235	805.6	60.4	0.74	1.73
		345	1018.1	71.0	1.07	1.96
		390	1080.1	72.3	2.98	4.11
	$\alpha$	0.05	749.3	55.3	0.95	1.07
0.1		1018.1	71.0	1.07	1.96	
0.15		1241.7	78.9	3.27	3.78	
0.2		1415.1	93.4	3.99	4.32	
Square	$\lambda$	20	1237.5	115.2	8.76	9.17
		40	857.3	52.5	1.56	2.54
		60	500.7	17.0	1.02	1.35
		80	324.1	5.9	0.73	0.96
	$n$	0.1	1009.5	85.2	1.41	8.18
		0.3	1031.4	80.7	1.85	3.54
		0.5	959.7	62.8	2.55	2.87
		0.7	725.8	53.2	2.68	2.69

#### 4. Mechanism analysis

The analytical results on monotonic  $P - \Delta$  relationship of circular RACFST beam-columns are presented to reveal the mechanism of such composite members. In this part, the sides with increasing and decreasing stress are considered as compressive and tensile zone, and the tensile and compressive stresses are treated as positive and negative, respectively.

Fig. 12 shows the typical monotonic  $P - \Delta$  curve of a RACFST beam-column. It can be found that, at point A, the maximum compressive stress of steel is about 80 percentage of the yield

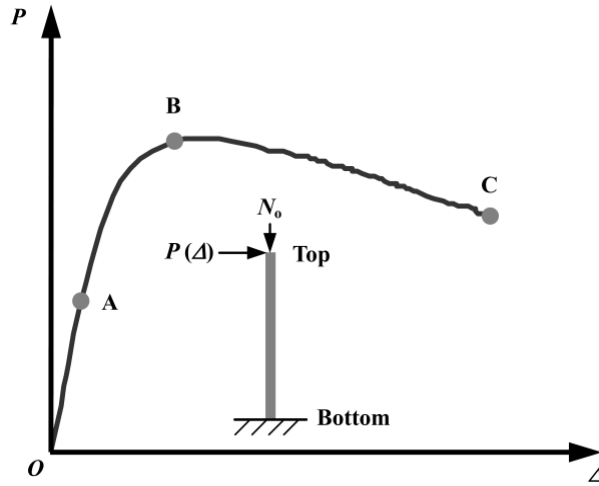


Fig. 12 Typical monotonic  $P - \Delta$  curve of a RACFST beam-column

strength of steel ( $f_y$ ). The lateral load at point B is equal to the lateral bearing capacity ( $P_u$ ). At point C, the lateral displacement at the free end equals to 100 mm. The stress distributions at points A to C are analyzed to reveal the mechanism of RACFST beam-columns under the entire loading process.

The distribution of longitudinal stresses of core RAC at the bottom end section is demonstrated in Fig. 13. It can be seen that, the tensile zone of concrete increases with increase of lateral displacement, and part of the compressive stress is greater than  $f'_{c,r}$  ( $= 44.88$  MPa) at point B. The maximum compressive stress at point C is larger than that at point B. This indicates that the stress of core RAC can increase even at the descending stage of  $P - \Delta$  curve.

Fig. 14 illustrates the longitudinal stresses of core RAC along the height. It can be observed that, at different loading stages, the maximum longitudinal stresses all appear at the bottom end section and the stresses gradually decrease from bottom to top end.

Fig. 15 shows the Mises stresses of steel tube at the aforementioned points. It can be seen that, the variation rules of steel stress along the height are similar to those of concrete stress. At point A, the steel stress of compressive zone is about  $0.8f_y$  and the stress of tensile zone is relatively small.

At point B, the maximum stress of compressive and tensile zone is equal to the yield strength; however, the yielding area of compressive zone is obviously larger than that of tensile zone

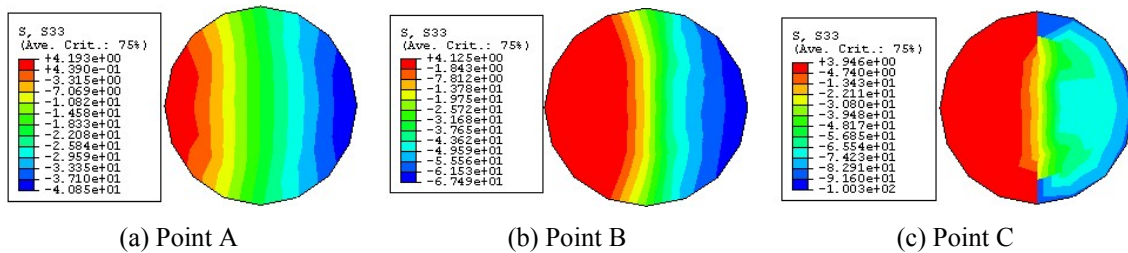


Fig. 13 Distribution of longitudinal stresses of core RAC

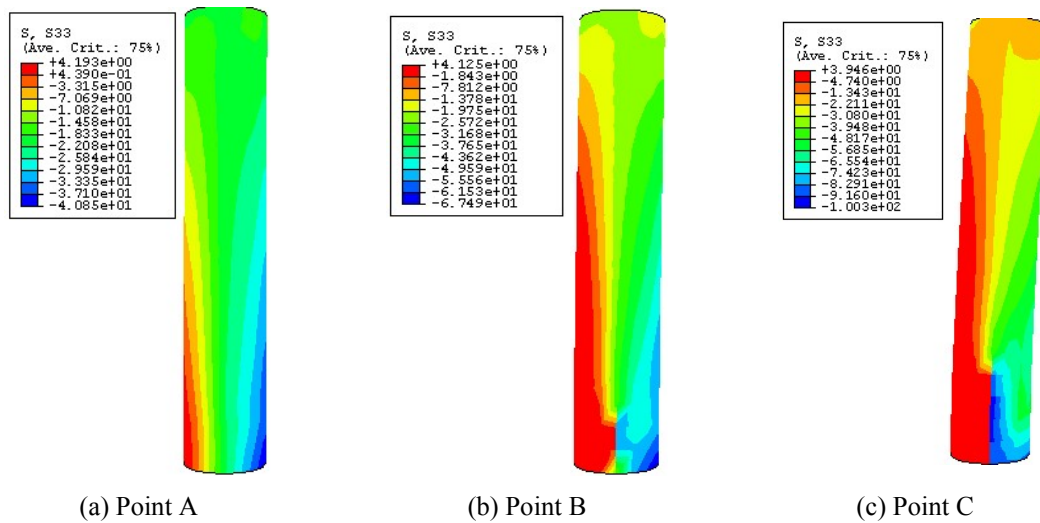


Fig. 14 Longitudinal stresses of core RAC along the height

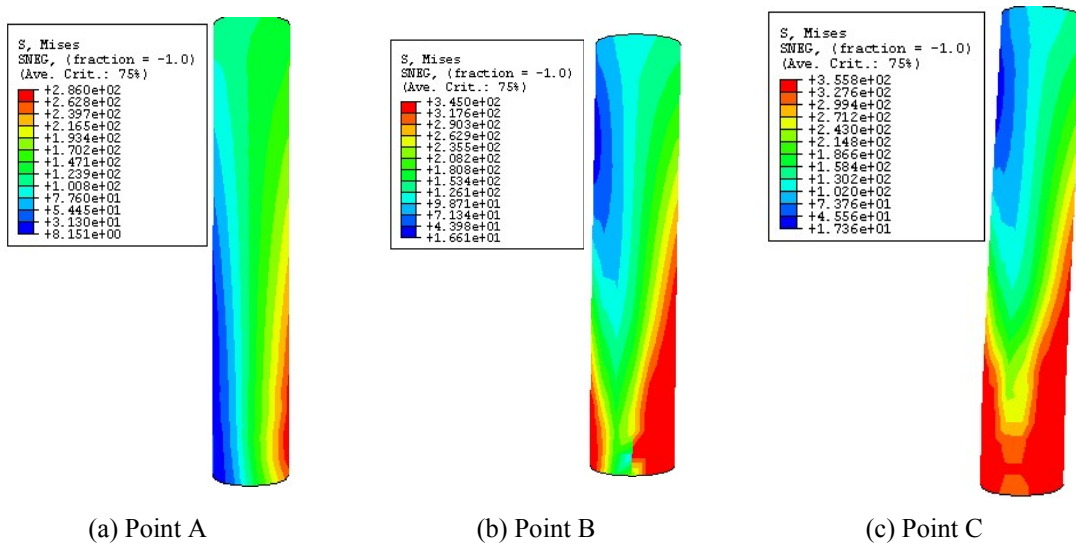


Fig. 15 Mises stresses of steel tube

owing to the existence of axial compressive load. At point C, the redistribution of the stresses occurs due to the plasticity developed at the bottom end.

Fig. 16 illustrates the  $p - \Delta$  relationship at different positions of the bottom end section, where  $p$  is the interaction stress between steel tube and core concrete. It can be seen that the interaction is always present in compression zone under the entire loading process. Generally,  $p$  increases with increase of lateral displacement and  $p$  of compression zone is larger than that of tensile zone.

The effect of typical parameters on  $p - \Delta$  relationship is shown in Fig. 17, where the thin and thick lines represent  $p$  at positions 1 and 3, respectively. It can be seen, the changing rules of  $p$  at different loading stage are not consistent and the difference of  $p - \Delta$  curves increases with increase

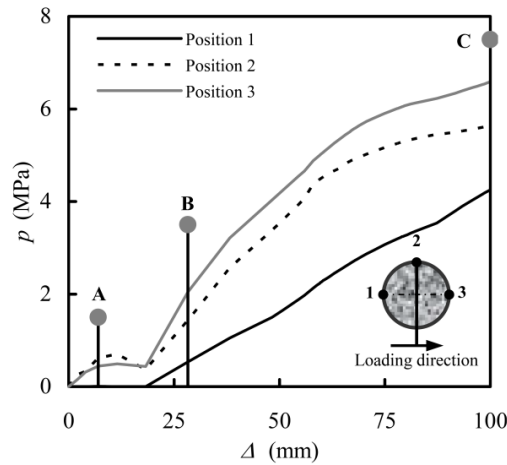


Fig. 16  $p - \Delta$  relationship at different positions

of lateral displacement under different parameters. The calculated interaction stresses at positions 1 and 3 while achieving the lateral bearing capacity ( $p_{B,1}$  and  $p_{B,3}$ ) are presented in Table 2. It is shown that,  $p_{B,1}$  and  $p_{B,3}$  increase with increase of  $f_y$  and  $\alpha$  and decrease of  $\lambda$ , and  $r$  and  $f'_c$  have a moderate effect on  $p_{B,1}$  and  $p_{B,3}$ . However,  $n$  has a reverse influence on  $p_{B,1}$  and  $p_{B,3}$ , i.e.,  $p_{B,1}$  increases and  $p_{B,3}$  decreases with increase of  $n$ .

## 5. Conclusions

Based on the limited studies presented in the paper, the following observations and conclusions can be drawn:

- A finite element analysis (FEA) model to predict the load versus deformation relationship, lateral bearing capacity and failure pattern of RACFST beam-columns under constant axial compressive load and cyclically increasing flexural loading has been developed, and generally the predicted results agree well with the measured results.
- Parametric analysis is carried out on  $P - \Delta$  and  $p - \Delta$  relationship, and it is shown that  $f_y$ ,  $\alpha$ ,  $\lambda$  and  $n$  are the important parameters to determine the behaviour of RACFST beam-columns under cyclic loading.
- While achieving lateral bearing capacity of RACFST beam-columns, the maximum longitudinal stress of core RAC is higher than  $f'_{c,r}$  and the maximum Mises stress of steel equals to  $f_y$ .
- Under the entire loading process of RACFST beam-columns under cyclic loading,  $p$  of compressive zone is larger than that of tensile zone.

## Acknowledgments

The research described in this paper was financially supported by the National Natural Science Foundation of China (No. 51421064), the Natural Science Foundation of Liaoning Province

(2013020125) and the Fundamental Research Funds for the Central Universities (DUT12ZD215). The financial support is gratefully acknowledged. The author also wishes to thank Mr. Lin-Tao Zhu for his assistance in the tests.

## References

- ABAQUS (2007), *ABAQUS Standard User's Manual*, Version 6.7, Dassault Systèmes Corp., Providence, RI, USA.
- Abdel-Rahman, N. and Sivakumaran, K.S. (1997), "Material properties models for analysis of cold-formed steel members", *ASCE J. Struct. Eng.*, **123**(9), 1135-1143.
- Aval, S.B.B., Saadeghvaziri, M.A. and Golafshani, A.A. (2002), "Comprehensive composite inelastic fiber element for cyclic analysis of concrete-filled steel tube columns", *ASCE J. Eng. Mech.*, **128**(4), 428-437.
- Birtel, V. and Mark, P. (2006), "Parameterised finite element modelling of RC beam shear failure", *Proceedings of 2006 ABAQUS Users' Conference*, Cambridge, MA, USA, May, pp. 95-108.
- Chung, K. (2010), "Prediction of pre- and post-peak behavior of concrete-filled circular steel tube columns under cyclic loads using fiber element method", *Thin-Wall. Struct.*, **48**(2), 169-178.
- EN 1992-1-1 (2004), Eurocode 2: Design of concrete structures – Part 1-1: General rules and rules for buildings, European Committee for Standardization, Brussels, Belgium.
- Hajjar, J.F., Molodan, A. and Schiler, P.H. (1998), "A distributed plasticity model for cyclic analysis of concrete-filled steel tube beam-columns and composite frames", *Eng. Struct.*, **20**(4-6), 398-412.
- Han, L.H. and Yang, Y.F. (2005), "Cyclic performance of concrete-filled steel CHS columns under flexural loading", *J. Const. Steel Res.*, **61**(4), 423-452.
- Han, L.H., Yang, Y.F. and Tao, Z. (2003), "Concrete-filled thin-walled steel SHS and RHS beam-columns subjected to cyclic loading", *Thin-Wall. Struct.*, **41**(9), 801-833.
- Han, L.H., Yao, G.H. and Tao, Z. (2007), "Performance of concrete-filled thin-walled steel tubes under pure torsion", *Thin-Wall. Struct.*, **45**(1), 24-36.
- Han, L.H., Liu, W. and Yang, Y.F. (2008), "Behaviour of concrete-filled steel tubular stub columns subjected to axially local compression", *J. Const. Steel Res.*, **64**(4), 377-387.
- Konno, K., Sato, Y., Kakuta, Y. and Ohira, M. (1997), "The property of recycled concrete column encased by steel tube subjected to axial compression", *T. Jpn. Concrete Inst.*, **19**(2), 231-238.
- Konno, K., Sato, Y., Ueda, T. and Onaga, M. (1998), "Mechanical property of recycled concrete under lateral confinement", *T. Jpn. Concrete Inst.*, **20**(3), 287-292.
- Mohanraj, E.K., Kandasamy, S. and Malathy, R. (2011), "Behaviour of steel tubular stub and slender columns filled with concrete using recycled aggregates", *J. South Af. Inst. Civil Eng.*, **53**(2), 31-38.
- Susantha, K.A.S., Ge, H. and Usami, T. (2002), "Cyclic analysis and capacity prediction of concrete-filled steel box columns", *Earthq. Eng. Struct. Dyn.*, **31**(2), 195-216.
- Valipour, H.R. and Foster, S.J. (2010), "Nonlinear static and cyclic analysis of concrete-filled steel columns", *J. Const. Steel Res.*, **66**(6), 793-802.
- Varma, A.H., Ricles, J.M., Sause, R. and Lu, L.W. (2002), "Seismic behavior and modeling of high-strength composite concrete-filled steel tube (CFT) beam-columns", *J. Const. Steel Res.*, **58**(5-8), 725-758.
- Varma, A.H., Sause, R., Ricles, J.M. and Li, Q. (2005), "Development and validation of fiber model for high-strength square concrete-filled steel tube beam-columns", *ACI Struct. J.*, **102**(1), 73-84.
- Yang, Y.F. (2007), "Theoretical research on load-deformation relations of recycled aggregate concrete-filled steel tubular members", *Ind. Construct.*, **37**(12), 1-6. [In Chinese]
- Yang, Y.F. (2011), "Behaviour of recycled aggregate concrete-filled steel tubular columns under long-term sustained loads", *Adv. Struct. Eng.*, **14**(2), 189-206.
- Yang, Y.F. and Han, L.H. (2006a), "Compressive and flexural behaviour of recycled aggregate concrete filled steel tubes (RACFST) under short-term loadings", *Steel Compos. Struct., Int. J.*, **6**(3), 257-284.
- Yang, Y.F. and Han, L.H. (2006b), "Experimental behaviour of recycled aggregate concrete filled steel tubular columns", *J. Const. Steel Res.*, **62**(12), 1310-1324.

- Yang, Y.F. and Zhu, L.T. (2009), "Recycled aggregate concrete filled steel SHS beam-columns subjected to cyclic loading", *Steel Compos. Struct., Int. J.*, **9**(1), 19-38.
- Yang, Y.F., Han, L.H. and Wu, X. (2008), "Concrete shrinkage and creep in recycled aggregate concrete-filled steel tubes", *Adv. Struct. Eng.*, **11**(4), 383-396.
- Yang, Y.F., Han, L.H. and Zhu, L.T. (2009), "Experimental performance of recycled aggregate concrete-filled circular steel tubular columns subjected to cyclic flexural loadings", *Adv. Struct. Eng.*, **12**(2), 183-194.

CC